Migration through a small pore disrupts inactive chromatin organisation in neutrophil-like cells

Elsie C. Jacobson[1], Jo K. Perry[1], David S. Long[2,3], Ada L. Olins[4], Donald E. Olins[4], Bryon E. Wright[2], Mark H. Vickers[1], Justin M. O'Sullivan[1*]

[1] Liggins Institute, University of Auckland, New Zealand
[2]Auckland Bioengineering Institute, University of Auckland, New Zealand
[3]Department of Biomedical Engineering, Wichita State University, USA
[4]University of New England, College of Pharmacy, Department of Pharmaceutical Sciences, Portland, ME, USA

* corresponding author: justin.osullivan@auckland.ac.nz

Author email addresses:ECJ <e.jacobson@auckland.ac.nz>, JKP <j.perry@auckland.ac.nz>, DSL <david.long@wichita.edu>, ALO <aolins@une.edu>, DEO <dolins@une.edu>, BEW <b.wright@auckland.ac.nz>, MHV <m.vickers@auckland.ac.nz>, JMO <justin.osullivan@auckland.ac.nz>

Keywords
Migration, heterochromatin, transcription, chromatin conformation, epigenetics, mechanotransduction, neutrophil, immune, Hi-C, nuclear remodeling.

Abstract

Mammalian cells are flexible and can rapidly change shape when they contract, adhere, or migrate. Their nucleus must be stiff enough to withstand cytoskeletal forces, but flexible enough to remodel as the cell changes shape. This is particularly important for cells migrating through constricted space, where the nuclear shape must change in order to fit through. This occurs many times in the life cycle of a neutrophil, which must protect its chromatin from damage and disruption associated with migration.

Total RNA-sequencing identified that neutrophil migration through 5 or 14 µm pores was associated with changes in the transcript levels of inflammation and chemotaxis-related genes, when compared to unmigrated cells. Differentially expressed transcripts specific to migration with constriction were enriched for groups of genes associated with cytoskeletal remodeling.

Hi-C was used to capture the genome organisation in control and migrated cells. Chromatin did not switch between the active (A) and inactive (B) compartments after migration. However, global depletion of mid- to long-range contacts was observed following active migration through the 5 µm pores. Chromatin contacts that decreased in frequency were enriched in inactive chromatin.

Mid- to long-range contacts are preferentially lost within inactive chromatin, thus protecting transcriptionally active contacts from the disruptive effects of migration with constriction. This is consistent with current hypotheses implicating heterochromatin as the mechanoresponsive form of chromatin. Further investigation concerning the contribution of heterochromatin to stiffness, flexibility, and protection of nuclear function will be important for understanding cell migration in human health and disease.

Background

Mammalian cells are subject to a wide range of mechanical environments and processes, including fluid shear stress [1], matrix stiffness [2], and migration [3]. Mounting an appropriate response to these stimuli is crucial for blood vessel development [1], cardiac health [4], muscle tone [5], bone strength [6], and the immune response [7]. Dysfunctional responses can lead to a wide range of diseases [8].

Cells are mechanically connected to their surroundings by integrins and other mechanoresponsive cell surface proteins [9]. In turn, these mechanoresponsive cell surface proteins are connected to the cytoskeleton, which remodels in response to chemical and mechanical signalling (reviewed in [10]). Cytoskeletal remodeling controls the shape of the cell, the nucleus, and even chromatin organisation [11–13]. External mechanical signals pass directly to the nucleoskeleton [14] through the linker of nucleoskeleton and cytoskeleton (LINC) complex, which connects the cytoskeleton to the nucleus [15]. A major mechanoresponsive element of the nucleoskeleton is the nuclear lamina, a key structural element which forms a mesh around the inside of the nuclear envelope [16]. The mammalian lamina consists of two major forms of intermediate filament; A-type lamins (Lamin A and C) and B-type lamins (Lamin B1, B2) [17]. High levels of Lamin A/C result in a stiff nucleus [2,18,19], although it is becoming increasingly recognised that chromatin also contributes to nuclear mechanics [20,21]. Heterochromatin stiffens the nucleus [20], interacts preferentially with the nuclear lamina, [22] the LINC complex [23], and other nuclear envelope proteins [24] and is therefore believed to play a role in the mechanoresponsiveness of the nucleus [20,25].

There are many acute consequences of mechanically challenging the nucleus [26,27]. When endothelial cell nuclei are exposed to shear stress, the position and shape of the nuclei aligns with the direction of the shear stress [1]. This alignment extends to loci within the nucleus, which move in the direction of the force after exposure to shear stress for more than 30 minutes [28]. Shear or stiffness induces cytoplasmic to nuclear shuttling of transcriptional and chromatin remodeling proteins including yes-associated protein (YAP)/transcription coactivator with PDZ binding domain (TAZ) [29] and chromatin modifier histone deacetylase 3 (HDAC3) [12]. In response to acute, applied force, chromatin linearises [30,31] and becomes more transcriptionally active [31]. However nuclear remodeling that occurs during cell migration is associated with chromatin condensation, with chemically-induced decondensation reducing the rate of migration [25,32].

Migration through a constriction provides unique mechanical challenges [33]. Due to its size and stiffness the nucleus is the rate limiting step for size reduction [18,34], but it also provides a stiff internal surface for the cytoskeleton to ‘push’ on and generate force [35]. Nuclear positioning during migration is tightly controlled by the cytoskeleton, and it is usually kept towards the back of the cell [36]. However, the nucleus leads transendothelial migration in immune cells, with nuclear lobes ‘drilling’ between endothelial cells to increase the gap between them and allow the neutrophil to pass through [37,38].

The nucleus plays a critical structural role during migration through constricted space, yet the spatial organisation of DNA is critical for transcriptional regulation, [39] and neutrophils must retain the structural features that are required for normal gene expression. Heterochromatin is tightly packed, self-interacting, and tethered at the periphery of most cells, while transcriptionally active euchromatin is found towards the centre [40]. Within

these compartments, local clusters of DNA are formed by loop extrusion [41,42], increasing the interactions between enhancers and promoters that are found within each topologically associated domain (TAD) [43]. Beyond individual enhancer/promoter interactions [44], active genes and enhancers cluster together [45] around the transcriptional machinery [46]. While many studies have described chromatin reorganisation during differentiation and disease (for example, [47–49]), it is not known how genome organisation is affected by the acute shape changes that occur during migration through a constriction. Neutrophils are highly migratory cells, with features that may contribute to nuclear stability, including a lobed nucleus, low Lamin A, and high heterochromatin content [18,25,50].

Here, we investigated whether migration through a constriction has an acute impact on chromatin conformation and transcriptional activity using an *in vitro* cell migration model. Neutrophil-like HL-60/S4 cells were differentiated and migrated through 5 µm pores (constricted migration) or 14 µm pores (non-constricted migration). When the two migration conditions were compared to each other, and to unmigrated cells, RNA-seq identified a strong transcriptional response to migration, and additional effects due to constriction. Hi-C analysis demonstrates that global genome structure is maintained following constricted migration with local disruptive effects occurring preferentially in inactive chromatin.

Results

An in vitro migration model

To investigate the effects of acute cell shape change, we developed a simplified model of neutrophil migration. HL-60/S4 cells were differentiated into neutrophil-like cells using retinoic acid (HL-60/S4-RA) [51]. Differentiation was confirmed by flow cytometric analysis of the cells immunolabelled for the surface antigen CD11b immunolabelled cells, and identification of the characteristic lobed nuclei by microscopy (Additional file 1: Supplementary fig S1a and b). Cell viability was confirmed with flow cytometric analysis of annexin V immunolabelled and propidium iodide stained cells (Additional file 1: Supplementary fig S1c). HL-60/S4-RA cells were migrated through two pore sizes, 5 µm and 14 µm, to simulate migration with and without constriction (Fig 1a).

HL-60/S4-RA cells are approximately 7-8 µm in diameter [18] (Additional file 1: Supplementary fig S1d) and passed through the 14 µm pores rapidly. By contrast, the rate of migration through 5 µm pores was much slower, most likely due to the remodeling required for a cell to fit through a pore smaller than itself (Additional file 1: Supplementary fig S1e). Migration rate was unlikely to be affected by pore availability as electron microscopy confirmed that the 5 and 14 µm pores cover approximately 9% or 5% of the membrane surface, respectively (Additional file 1: Supplementary fig S2).

Transcriptional changes after migration and remodeling are distinct

We captured acute responses to migration with or without constriction by processing cells within 30 minutes post-migration. We contend that this model allows us to isolate the effects of passage through the transwell chamber from the effects of nuclear remodeling that resulted from constricted migration. We used total RNA-seq to identify genes that were differentially expressed, comparing unmigrated control cells with cells that migrated through 5 µm or 14 µm pores. This enabled us to identify changes in steady-state total RNA levels associated

with migration per se, and to distinguish them from transcriptional changes specific to migration with constriction.

The majority of observed migration-induced gene expression changes fell into one of three sets (Additional file 2: Supplementary table S1). The first set included 420 genes with highly correlated fold changes (R^2=0.92, $p < 2.2e^{-16}$, Fig 2a and b) following migration through 5 µm or 14 µm pores, when compared to unmigrated control cells. We consider this set of genes to reflect the effects of passage through the migration chamber. Gene ontology (GO) analysis, using TopGo [52], identified enrichment for GO biological process terms that included response to cytokine (FDR adjusted $p = 4.06e^{-05}$, Fisher's exact test) and monocyte chemotaxis (FDR adjusted p = 0.044, Fisher's exact test; Additional file 3: Supplementary table S2). This suggested that the environment of the migration chamber was sufficient to stimulate immune-like transcriptional responses in these neutrophil-like cells, despite the lack of added chemoattractants, and 14 µm diameter pores being substantially larger than the 7 µm diameter cells [18] (Additional file 1: Supplementary fig S1d).

The second set contained 1433 genes that were significantly differentially expressed after migration through 5 µm pores, when compared to unmigrated control cells. The genes within this group were not significantly differentially expressed following migration through 14 µm pores. However, the highly correlated fold changes (R^2=0.82, $p < 2.2e^{-16}$, Fig 2a and c) indicated that the change in RNA transcript levels following migration with constriction was in the same direction, but with larger effect sizes, following migration with constriction. GO analysis identified enrichment for terms, including inflammatory response (FDR adjusted p = 0.004, Fisher's exact test) and chemokine mediated signalling pathway (FDR adjusted p = 0.011, Fisher's exact test) (Additional file 3: Supplementary table S3).

The third set of 199 genes exhibited differential transcript levels following migration through 5 µm pores when compared to either 14 µm pores or control cells. There was a low correlation between the transcript levels of these genes following migration through the two pore sizes, compared to unmigrated cells (R^2=0.32, $p < 2.2e^{-16}$, Fig 2a and d). Therefore, this set represents the transcript changes that were specific to the constriction aspect of the assay. GO analysis demonstrated that genes associated with distinct biological processes were regulated in the cells migrated with constriction. Seventeen genes were involved with actin cytoskeleton remodeling (FDR adjusted p = 0.071, Fisher's exact test) (Additional file 3: Supplementary table S4). In addition, migration through 5 µm pores was associated with changes in transcript levels of genes with molecular function associated with lactate transport (FDR adjusted p = 0.025, Fisher's exact test), and Rab GTPase activity (FDR adjusted p = 0.086, Fisher's exact test) (Additional file 3: Supplementary table S5).

Collectively, the results of the total RNA-seq were consistent with migration through either pore size being associated with changes in transcript levels for genes associated with inflammation and chemotaxis. Moreover, migration with constriction was associated with changes in transcript levels of cytoskeleton remodeling genes.

Genome organisation is robust to migration

We used Hi-C to investigate global features of genome organisation, to determine whether migration induced remodeling at different levels of nuclear structure. Heterochromatin preferentially interacts with itself, forming a phase separated compartment isolated from euchromatin [40,53]. Distinct interaction patterns can be extracted from the Hi-C heatmap

using principle component analysis, allowing us to assign regions of DNA to either the active (A) or inactive (B) compartment, which generally corresponds to euchromatin and heterochromatin respectively [54]. Compartments were identified in HOMER [55] at 300 kb resolution (500 kb super-resolution), and correlation matrices of migrated and unmigrated cells were compared directly in order to identify regions that showed opposite interaction patterns between conditions. Overall, the compartment structure was stable after migration with or without constriction (Fig 3a). Following migration with constriction, four bins switched compartment, while none switched after migration without constriction ($R<0$ (anticorrelated), Pearson correlation coefficient, Additional file 4: Supplementary table S6). However, there were no differentially expressed genes in the switched regions.

Regions of chromatin that are close in linear space are more likely to come into contact than those that are further apart [54], but the rate of degradation of contact frequency across distance can vary. For instance, during neutrophil differentiation chromatin undergoes supercoiling, resulting in a loss of contacts below 3 Mb apart, and an increase in long range contacts above 3 Mb [47]. After migration with constriction we observe a depletion of contacts particularly between 100 kb and 5 Mb, indicating widespread disruption of mid- to long-range contacts (Fig 3b).

TADs are conserved units of DNA organisation characterised by increased chromatin contacts within the region [56]. Due to the loss of mid- to long-range contacts after migration, contact frequencies both within and between TADs decreased significantly following migration with constriction. Contact frequencies also decreased significantly after migration without constriction, but the effect size was smaller (Additional file 1: Supplementary fig. 3a). However, TAD size was conserved between samples (Additional file 1: Supplementary fig. 3b), and the majority of TADs identified in the migrated samples were ≥80% overlapping with TADs identified in the control sample (Additional file 1: Supplementary fig. 3c).

Our results indicate that the two major features of genome organisation, compartments (A and B) and topologically associated domains (TADs), were conserved after migration with or without constriction. However, mid- to long-range contacts within these structural features were disrupted following migration with constriction.

Transcriptionally active DNA is protected from remodeling

The disruption of mid to long-range contacts led us to identify total and differential contacts at 40 kb resolution (100 kb super-resolution) between loci 100 kb to 5 Mb apart, where the difference in contact frequency depletion is most pronounced.

HOMER [55] was used to identify significant contacts ($FDR<0.05$) and to compare normalised contact frequencies between migrated and unmigrated cells. There were 586 contacts that significantly decreased frequency ($FDR<0.1$, Fig 4a) between cells that were migrated with constriction compared to control. Few contacts changed frequency between unmigrated cells and those migrated without constriction (Fig 4a). Therefore, all further analyses were performed on the set of contacts that decreased in frequency following migration with constriction.

Identifying contacts at 100 kb resolution prevented us from identifying individual promoter-enhancer contacts. Therefore, we investigated whether contacts were more likely to be disrupted in active or inactive regions of the genome following migration with constriction.

There were a similar number of total contacts in compartments A and B (Additional file 1: Supplementary fig 3d), but more than two times the numbers of disrupted contacts in compartment B (Additional file 1: Supplementary fig 3e). Bootstrapping confirmed the observation that there was a highly significant depletion of disrupted contacts in compartment A (Fig 4b, $p < 0.0001$). To test this result orthogonally, we identified 173 bins, 300 kb in size, with a low correlation between migration with constriction and unmigrated cells ($R<0.5$, Additional file 4: Supplementary table S6). Only 39 of these regions were in compartment A, significantly fewer than expected by chance (Fig 4c, $p < 1e^{-21}$, bootstrapping). Combined, these data show that disruption preferentially occurs in compartment B, and is less likely to be located in active regions of the genome.

We investigated transcriptional activity in the migration dependent disrupted regions. Firstly, we intersected genes whose transcripts were differentially expressed between migration with and without constriction, and found no enrichment when compared to randomly selected expressed genes in disrupted contacts (Fig 4d). We then calculated the density of expressed genes in total and disrupted contacts in compartments A and B. There was a lower density of expressed genes in compartment B as expected, and also significantly fewer expressed genes in disrupted contacts in either compartment ($p<0.0001$, two-proportions z-test) (Fig 4e). We also observed that the median transcript level of expressed genes was significantly lower in disrupted contacts than significant contacts ($p<0.05$, bootstrapping) (Fig 4f). An example region on chromosome 17 shows the loss of chromatin contacts particularly occurring in a transcriptionally inactive locus in compartment B (Fig 5). This is consistent with transcriptionally active chromatin contacts being protected from the disruptive effects of cell migration through a small pore.

Of the 247 genes identified in disrupted contacts (Additional file 5: Supplementary table S7), 197 were protein coding and six of these were differentially expressed between migration with and without constriction (*KCNJ15*, *AGAP3*, *ARRDC2*, *FAM46A*, and *MICAL2*). However, because we analysed cells within 30 minutes of migration, slower changes related to contact disruptions may not have been detected. Therefore, we looked for enrichment of gene ontology terms in the full set of 197 protein coding genes; but found no significant enrichments (FDR<0.1) in either biological processes or molecular function.

Collectively our results demonstrate that disrupted contacts were depleted in active chromatin and not associated with differential gene expression. This is consistent with transcriptionally active chromatin being protected from disruption during migration.

Discussion

Our simplified model of migration successfully isolated the effects of passage through the migration chamber from those associated with cell and nuclear remodeling. The induction of inflammatory, chemotaxis, and proliferative genes in cells that had migrated through large pores supports both the validity of our migration model, and roles for crowding [57] and fluid shear [58] in neutrophil activation.

Remodeling-specific changes associated with constricted migration were enriched for genes involved in energy intake, specifically the pyruvate and lactate transporters *SLC16A7* [59] and *SLC16A3* [60]. Anaerobic glycolysis, which produces ATP via the glycolysis of pyruvate to lactate, is the neutrophils' main form of ATP generation [61]. Cytoskeleton remodeling is energy intensive, and lactate production has the inevitable side effect of acid production [62].

Milieu acidification is a characteristic of inflammatory sites [63], and may be a direct consequence of energy intensive migration. Intriguingly, metastatic cancer cells also rely on aerobic glycolysis for movement, despite also generating ATP via mitochondrial respiration [64].

Transcript levels of the Rab GTPases also changed with constricted migration-associated remodeling. The Rab GTPases are associated with vesicle mobilisation [65], which is a critical part of the neutrophil immune response [66,67]. Granule exocytosis is also regulated by adherence [68,69], cytoskeleton remodeling [70], and migration [71], supporting a role of cell shape change and mechanotransduction in priming neutrophil antibacterial responses.

Recent studies have shown that heterochromatin forms a phase-separated compartment within the nucleus [53,72]. These heterochromatic phases act like viscous 'droplets', and therefore should remain demixed as the nucleus changes shape [73]. Our results support this model as the widespread disruption of mid- to long-range contacts is not reflected in changes to the compartmentalisation of the nucleus. Instead the heterochromatin spatial organisation is altered in response to nuclear shape change [25], possibly in order to protect damage and disruption to the organisation of transcriptionally active euchromatin. Under this model, the multiple lobes of the neutrophil nucleus would provide a larger surface area and therefore increased force dispersion.

Neutrophils have a very low Lamin A content [18], and therefore would be expected to undergo a lower rate of nuclear rupture, but a faster death due to DNA damage, based on recent studies by Denais and Raab [74,75]. However chromatin composition contributes strongly to the mechanical properties of the nucleus [20], and the high levels of heterochromatin along with the increased force dispersion could compensate for the lack of Lamin A in the nuclear envelope. Neutrophil differentiation is associated with an increase of long range contacts (>3 Mb) in compartment B [47]. The switch between short and long range contacts is not associated with transcriptional changes, indicating a structural role [47]. Indeed, the supercoiling of heterochromatin could contribute to its force absorbing properties during migration.

Microscopy of aspirated nuclei and magnetically twisted cells has shown that chromatin linearizes as the nucleus stretches [30,31]. These studies focussed on loci that were a repetitive region[30] and a bacterial artificial chromosome [31]. Therefore, it is likely that these loci were located in the heterochromatic phase. Euchromatic loci may prove to be less malleable, although we would expect to see linearization to some extent, just as we did see some disrupted contacts in active chromatin.

The enrichment of disrupted contacts in transcriptionally inactive loci even within compartment A leads us to believe that migration-associated chromatin remodeling is not a major contributor to gene regulation. However, we were not able to identify specific promoter-enhancer contacts due to the resolution of the Hi-C data. Promoter-capture Hi-C [76] after migration may reveal a finer level of chromatin remodeling in response to nuclear shape change. Nascent RNA-sequencing would also provide more accurate measures of transcriptional activity, as total RNA-sequencing captures the result of both RNA production and degradation [77]. Moreover, the spatial organisation and transcriptome may have different characteristics at different time points after migration. The acute changes may activate pathways and feedback loops and result in stable changes in gene expression. Alternatively, continued migration (such as through the interstitial space) may be necessary

to retain the transcriptional signature of a migrated cell. The stability of the chromatin contact changes is also unknown. As such, the disruption of mid- to long-range contacts observed after 30 minutes may reflect a 'recovering' nucleus that is converging on the unmigrated cell structure, or a 'remodeling' nucleus that is in the process of gaining a distinct nuclear structure.

All cells in the human body must make a compromise between stiffness and flexibility of the nucleus, which is controlled by the nucleoskeleton and chromatin composition[20]. Migration through a constriction is an excellent model for this compromise, as it requires resistance to mechanical forces generated by the cytoskeleton, yet the nucleus must change shape. The stiff nuclei of cancer cells rupture during migration, but lowering Lamin A levels to decrease stiffness leads to increased cell death [74,75]. Similarly, loss or mutation of Lamin A leads to muscular dystrophy and cardiac failure [4,78], as muscle nuclei are unable to survive the repeated force of contraction. However, extreme stiffness also causes cardiac dysfunction [79,80]. Lamin A is evenly distributed across the nuclear periphery and therefore nuclear lamina stiffness is consistent across the nucleus. In contrast, it is possible for chromatin to form stiff 'foci' for the cytoskeleton to push against [25], while remaining flexible to allow shape change. Thus, chromatin may alleviate the loss of Lamin A protection in nuclei that undergo force-induced shape change.

The mechanisms that interact to confer nuclear properties during mechanical stress are likely to be complex and partially redundant. For instance, knockdown of SUN1, a semi-redundant component of the LINC complex [81], rescues Lamin A knockout mice from Emery-Dreifuss muscular dystrophy [82]. Notably, granulocytic HL-60/S4 cells have low levels of SUN1 [83], which may contribute to their enhanced survival compared to Lamin A knockout cells [74,75]. Taking an integrative approach to studying nuclear mechanics is not trivial. However, understanding the interplay between Lamin A, heterochromatin, SUN1, and other nuclear components remains an important frontier in cells undergoing migration and contraction during neuronal development, bone healing, cardiovascular function, skeletal muscle growth, and the immune response.

Conclusion

We have shown that nuclear remodeling during constricted migration disproportionally disrupts inactive chromatin, possibly protecting transcriptionally active chromatin and minimising transcriptional dysregulation during migration. Our study contributes to the growing understanding of heterochromatin as a key player in the structure and mechanosensitivity of the nucleus.

Methods

Cell culture

HL-60/S4 cells (available from ATCC #CCL-3306) were cultured at 37°C, 5% CO_2 in RPMI 1640 (ThermoFisher) supplemented with 10% fetal bovine serum (Moregate Biotech), 1% penicillin/streptomycin (ThermoFisher), and 1% GlutaMAX^{TM} (ThermoFisher). Cells were differentiated into a granulocytic phenotype with 1 µM all trans retinoic acid (ATRA) dissolved in ethanol (Sigma Aldrich) for four days as previously described [51,84]. To

visualise nuclear morphology, cells were cytospun at 500 rpm for 5 minutes onto slides, then stained with Wright-Giemsa (Sigma-Aldrich).

Flow Cytometry

Flow cytometry analysis of the cell surface antigen, CD11b, was performed as described previously [18]. Briefly, 10^6 cells were washed in PBS, blocked with human IgG (Sigma-Aldrich), then incubated with Alexa Fluor 700 Mouse Anti-Human-CD11b for 30 minutes. The proportion of live/dead/apoptotic cells was assessed with the Alexa Fluor® 488 annexin V/Dead Cell Apoptosis Kit with Alexa Fluor® 488 annexin V and PI (ThermoFisher). Briefly, $5x10^5$ cells were washed and incubated with Alexa Fluor® 488 annexin V and 100 µg/mL PI for 15 minutes. Fluorescence was measured with a FACSAria II SORP cell sorter (BD Biosciences). Analysis was performed in FlowJo v10.

Migration

A Boyden chamber (NeuroProbe, BY312) was modified by cutting the chamber in half, leaving the upper and lower wells separated by a filter held in place by an acetal retainer. A trimmed p200 pipette tip was inserted in the opening of the lower well, and a hole was drilled on the opposite side of the lower well so a tube could be connected to a syringe. These modifications facilitated continuous flow of media through the lower well (Fig 1a). Migration assays were carried out in a hypoxic glove box (Coy Laboratory Products) at 37ºC, 5% CO_2, 20% O_2. Media was perfused at 0.2mL/min with a syringe pump (New Era Pump Systems, NE-1002X). Growth media was used in both upper and lower wells. Polycarbonate membranes with 5 µm diameter pores or 14 µm diameter pores (NeuroProbe) were imaged using scanning electron microscopy. Migrated cells were collected and processed for sequencing every 30 minutes for 3-4 hours (5 µm pores) or 1 hour (14 µm pores). Unmigrated control cells were processed for sequencing during the first 30 minutes of migration. All processed time points were pooled and frozen at -80°C prior to RNA extraction or Hi-C library preparation.

RNA sequencing

Cells were lysed in TRiZOL LS (Invitrogen) and phase separated with chloroform. At this point four 5µm migration assays were pooled per replicate in order to extract enough RNA for sequencing. RNA was extracted with the Qiagen RNeasy micro kit (Qiagen, 74004). RNA and lncRNA libraries were prepared by Annoroad Gene Technology Co., Ltd. (Beijing, China) using ribosomal RNA depletion with RiboZero Magnetic Gold Kit (Human/Mouse/Rat) and sequenced on the Illumina Hi-seq X 150PE.

Hi-C

Whole genome chromosome conformation capture (Hi-C) was performed as in [85] with restriction enzyme *Mbo*I (NEB).[85] Formaldehyde fixed cells from 4-5 migration assays were pooled to reach 2 million cells required. The library was prepared for Illumina sequencing with the TruSeq Nano kit (Truseq Nano DNA LT Sample Preparation Kit). One library was sequenced per lane of the Illumina HiSeq X 150PE.

RNA-seq analysis

Read quality was confirmed with FastQC v0.11.4. Reads were aligned to hg38 and gencode annotations v27 using STAR v2.5.3a with default settings. FeatureCounts v1.5.2 was used to aggregate transcripts for gene-level analysis and quantify the reads with GENCODE annotations v27 (Additional file 3: Supplementary table S8). Expressed genes were filtered using default settings in DEseq2 v1.16.1. PCA of variance stabilised transcripts confirmed clustering by condition (Additional file 1: Supplementary fig S4). Differentially expressed genes were identified at FDR<0.05 using DEseq2 v1.16.1. Gene ontology enrichments were calculated with TopGo v2.28.0 using the weight01 algorithm and the Fisher statistic. Categories containing <2 genes were filtered out, and p values adjusted for FDR.

Hi-C analysis

Read quality was confirmed with FastQC v0.11.4. Reads were aligned to hg38 and filtered using HiCUP v0.5.9 (Additional file 3: Supplementary table S9). High correlation between replicates was confirmed (R>0.994, Additional file 3: Supplementary table S10), then libraries were pooled and downsampled so that the three conditions (control, 5µm pores, 14µm pores) had the same number of valid reads (144,382,298). HiCUP output was converted to HOMER [55] input using the hicuptohomer script provided by HiCUP. Compartments were identified by performing PCA on each chromosome in HOMER v4.9.1 at 300kb resolution, 500kb super-resolution on a matrix normalised with the HOMER default. TSS locations were used to seed active regions to determine the correct sign of the PC1 value. Chromosomes were excluded from compartment analysis if the first principal component corresponded to the chromosomal arms (chromosomes 4,5,19,21,X). Correlation matrices were compared to identify compartment switching and compartment disruption with the getHiCcorrDiff.pl script provided by HOMER. Significant and differential contacts were identified in HOMER at 40 kb resolution, 100 kb super-resolution with default normalisation, minimum distance 100 kb, maximum distance 5 Mb. HOMER was also used to generate chromosomal matrices at 50 kb resolution for topologically associated domain (TAD) analysis in TopDom v0.0.2 using a window size of 5.

Figure Legends

Figure 1. Neutrophil-like cells were migrated through two sizes of porous membrane. a) A classical Boyden chamber was modified to allow a continuous flow of media (0.2 mL/min) through the lower well. Migrated cells were processed every thirty minutes. Three experimental conditions were used. b) Cells that did not migrate c) cells that migrated through pores larger than themselves (14 µm diameter) and d) cells that migrated through pores smaller than themselves (5 µm diameter).

Figure 2. Gene expression changes. a) Venn diagram of significantly differentially expressed genes (DESeq2, FDR<0.05) between 14 µm and 5 µm pores, unmigrated and 5 µm pores, unmigrated and 14 µm pores. 80% of the genes differentially expressed after migration through 14 µm pores also change after migration through 5µm pores. b) The 420 genes that changed in both conditions were highly correlated (R^2=0.92). Genes that were significant. c) While 1621 additional genes change expression after migration through 5 µm, only 178 of these were significantly different between the two pore sizes. The 1443 that were not significantly different are highly correlated changes compared to unmigrated cells (R^2=0.82). d) The relatively small subset of 199 genes are uniquely different after migration through 5 µm pores. We believe these genes are associated with the effects of remodeling and have low correlation (R^2=0.36) between 5 and 14 µm pore migration. e) Heatmap of remodeling

specific genes, as shown in d. Each column represents one sample, each row is one gene. Cells are coloured by counts normalised by library size and scaled within each row. Rows are clustered by heatmap.2 generated dendrogram in R.

Figure 3. Global genome structure a) Compartment switching did not occur after migration, the first principal component of the correlation matrix for chromosome two is shown here for i) unmigrated cells, ii) cells migrated through 14 µm pores, and iii) cells migrated through 5 µm pores. C) Comparison of distance dependent contact probability plots show a loss of contacts occurring mostly between 100 kb and 5 Mb after migration with constriction.

Figure 4. Features of differential contacts. a) Differential contacts 100 kb to 5 Mb apart were identified at 100 kb resolution. 568 contacts decreased in frequency after migration through 5 µm pores. The pool of significant contacts was sampled with replacement and intersected with genomic features to generate bootstrap distributions. Black lines indicate 95% of the distributions, and the red line shows the observed number of intersects. b) Disrupted contacts were significantly depleted for compartment A, indicating that heterochromatin was more affected by the disruptive effects of migration. c) 300 kb bins with low correlation of their intrachromosomal interaction profiles between migration with constriction and control ($R<0.5$, Pearson's correlation coefficient) were more likely to occur in compartment B ($p<1e^{-21}$, bootstrapping) d) There was no enrichment for remodeling specific genes (Fig 2D) in disrupted contacts. e) The average number of expressed genes per contact was lower in disrupted contacts than total contacts in both compartment A and B, suggesting that transcription may provide some protection from the effects of remodeling. f) The median gene expression of the 197 protein coding genes in disrupted contacts was significantly lower than the median gene expression of randomly selected genes in significant contacts.

Figure 5. Example of contact depletion occurring in a transcriptionally inactive region. a) significant contacts (FDR<0.1) in control cells, and cells migrated with or without constriction. b) Hi-C heatmap PC1 values, indicating compartment A (positive) and B (negative) in the three conditions. Although they are not visually identical, these bins are still positively correlated with each other (Additional file 4: Supplementary table S6). c) the position of expressed genes, and log mean gene expression of the two migration conditions. None of these genes are significantly differentially expressed between migration with and without constriction.

Bibliography

1 Steward R, Tambe D, Hardin CC, et al. Fluid shear, intercellular stress, and endothelial cell alignment. Am J Physiol - Cell Physiol 2015;308:C657–C664.

2 Engler AJ, Sen S, Sweeney HL, et al. Matrix elasticity directs stem cell lineage specification. Cell 2006;126:677–689.

3 Cao X, Moeendarbary E, Isermann P, et al. A chemomechanical model for nuclear morphology and stresses during cell transendothelial migration. Biophys J 2016;111:1541–1552.

4 Wolf CM, Wang L, Alcalai R, et al. Lamin A/C haploinsufficiency causes dilated cardiomyopathy and apoptosis-triggered cardiac conduction system disease. J Mol Cell Cardiol 2008;44:293–303.

5 Burkholder TJ. Mechanotransduction in skeletal muscle. Front Biosci 2007;12:174–191.

6 Seefried L, Ebert R, Müller-Deubert S, et al. Mechanotransduction in aging and

osteoporosis. Osteologie 2010;19:232–239.
7 Thauland TJ, Hu KH, Bruce MA, et al. Cytoskeletal adaptivity regulates T cell receptor signaling. Sci Signal 2017;10:eaah3737.
8 Ingber D. Mechanobiology and diseases of mechanotransduction. Ann Med 2003;35:564–577.
9 Jansen KA, Atherton P, Ballestrem C. Mechanotransduction at the cell-matrix interface. Semin Cell Dev Biol 2017;71:75–83.
10 Wang N. Review of Cellular Mechanotransduction. J Phys D Appl Phys 2017;50.
11 Uhler C, Shivashankar G V. Geometric control and modeling of genome reprogramming. Bioarchitecture 2016;6:76–84.
12 Jain N, Iyer K V., Kumar A, et al. Cell geometric constraints induce modular gene-expression patterns via redistribution of HDAC3 regulated by actomyosin contractility. Proc Natl Acad Sci 2013;110:11349–11354.
13 Ramdas NM, Shivashankar GV. Cytoskeletal control of nuclear morphology and chromatin organization. J Mol Biol 2015;427:695–706.
14 Dahl KN, Kalinowski A. Nucleoskeleton mechanics at a glance. J Cell Sci 2011;124:675–678.
15 Kim DI, Birendra KC, Roux KJ. Making the LINC: SUN and KASH protein interactions. Biol Chem 2015;396:295–310.
16 Dahl KN, Kahn SM, Wilson KL, et al. The nuclear envelope lamina network has elasticity and a compressibility limit suggestive of a molecular shock absorber. J Cell Sci 2004;117:4779–4786.
17 Aebi U, Cohn J, Buhle L, et al. The nuclear lamina is a meshwork of intermediate-type filaments. Nature 1986;323:560–564.
18 Rowat AC, Jaalouk DE, Zwerger M, et al. Nuclear envelope composition determines the ability of neutrophil-type cells to passage through micron-scale constrictions. J Biol Chem 2013;288:8610–8618.
19 Swift J, Ivanovska IL, Buxboim A, et al. Nuclear lamin-A scales with tissue stiffness and enhances matrix-directed differentiation. Science (80-) 2014;341:1240104.
20 Stephens AD, Banigan EJ, Adam SA, et al. Chromatin and lamin A determine two different mechanical response regimes of the cell nucleus. Mol Biol Cell 2017;28:1984–1996.
21 Stephens AD, Liu PZ, Banigan EJ, et al. Chromatin histone modifications and rigidity affect nuclear morphology independent of lamins. Mol Biol Cell 2018;29:220–233.
22 van Steensel B, Belmont AS. Lamina-associated domains: Links with chromosome architecture, heterochromatin, and gene repression. Cell 2017;169:780–791.
23 Poulet A, Duc C, Voisin M, et al. The LINC complex contributes to heterochromatin organisation and transcriptional gene silencing in plants. J Cell Sci 2017;130:590–601.
24 Le HQ, Ghatak S, Yeung C-YC, et al. Mechanical regulation of transcription controls Polycomb-mediated gene silencing during lineage commitment. Nat Cell Biol 2016;18:864–875.
25 Gerlitz G, Bustin M. Efficient cell migration requires global chromatin condensation. J Cell Sci 2010;123:2207–2217.
26 Miroshnikova YA, Nava MM, Wickstro M SA. Emerging roles of mechanical forces in chromatin regulation.
27 Kirby TJ, Lammerding J. Emerging views of the nucleus as a cellular mechanosensor. Nat Cell Biol 2018;20:373–381.
28 Booth-Gauthier EAA, Alcoser TAA, Yang G, et al. Force-induced changes in subnuclear movement and rheology. Biophys J 2012;103:2423–2431.
29 Dupont S, Morsut L, Aragona M, et al. Role of YAP/TAZ in mechanotransduction.

Nature 2011;474:179–183.
30 Irianto J, Xia Y, Pfeifer CR, et al. As a nucleus enters a small pore, chromatin stretches and maintains integrity, even with DNA breaks. Biophys J 2017;112:446–449.
31 Tajik A, Zhang Y, Wei F, et al. Transcription upregulation via force-induced direct stretching of chromatin. Nat Mater 2016.
32 Gerlitz G, Bustin M. The role of chromatin structure in cell migration. Trends Cell Biol 2011;21:6–11.
33 Calero-Cuenca FJ, Janota CS, Gomes ER. Dealing with the nucleus during cell migration. Curr Opin Cell Biol 2018;50:35–41.
34 Davidson PM, Denais C, Bakshi MC, et al. Nuclear deformability constitutes a rate-limiting step during cell migration in 3-D environments. Cell Mol Bioeng 2014;7:293–306.
35 Graham DM, Andersen T, Sharek L, et al. Enucleated cells reveal differential roles of the nucleus in cell migration, polarity, and mechanotransduction. J Cell Biol 2018;217:895–914.
36 Friedl P, Wolf K, Lammerding J. Nuclear mechanics during cell migration. Curr Opin Cell Biol 2011;23:55–64.
37 Barzilai S, Yadav SK, Morrell S, et al. Leukocytes breach endothelial barriers by insertion of nuclear lobes and disassembly of endothelial actin filaments. Cell Rep 2017;18:685–699.
38 Feng D, Nagy JA, Pyne K, et al. Neutrophils emigrate from venules by a transendothelial cell pathway in response to FMLP. J Exp Med 1998;187:903–915.
39 Rennie S, Dalby M, van Duin L, et al. Transcriptional decomposition reveals active chromatin architectures and cell specific regulatory interactions. Nat Commun 2018;9:487.
40 Falk M, Feodorova Y, Naumova N, et al. Heterochromatin drives organization of conventional and inverted nuclei. bioRxiv 2018:244038.
41 Fudenberg G, Abdennur N, Imakaev M, et al. Emerging evidence of chromosome folding by loop extrusion. bioRxiv 2018:264648.
42 Ganji M, Shaltiel IA, Bisht S, et al. Real-time imaging of DNA loop extrusion by condensin. Science 2018;360:102–105.
43 Dixon JR, Selvaraj S, Yue F, et al. Topological domains in mammalian genomes identified by analysis of chromatin interactions. Nature 2012;485:376–380.
44 Sanyal A, Lajoie B, Jain G, et al. The long-range interaction landscape of gene promoters. Nature 2012;489:109–113.
45 Beagrie RA, Scialdone A, Schueler M, et al. Complex multi-enhancer contacts captured by genome architecture mapping. Nature 2017;543:519–524.
46 Hnisz D, Shrinivas K, Young RA, et al. A phase separation model for transcriptional control. Cell 2017;169:13–23.
47 Zhu Y, Gong K, Denholtz M, et al. Comprehensive characterization of neutrophil genome topology. Genes Dev 2017;31:141–153.
48 Krijger PHL, Di Stefano B, de Wit E, et al. Cell-of-origin-specific 3D genome structure acquired during somatic cell reprogramming. Cell Stem Cell 2016;18:597–610.
49 Rosa-Garrido M, Chapski DJ, Schmitt AD, et al. High-resolution mapping of chromatin conformation in cardiac myocytes reveals structural remodeling of the epigenome in heart failure. Circulation 2017;136:1613–1625.
50 Skinner BM, Johnson EEP. Nuclear morphologies: their diversity and functional relevance. Chromosoma 2017;126:195–212.
51 Olins AL, Buendia B, Herrmann H, et al. Retinoic acid induction of nuclear envelope-

limited chromatin sheets in HL-60. Exp Cell Res 1998;245:91–104.
52 Alexa A, Rahnenfuhrer J. topGO: Enrichment analysis for gene ontology 2016.
53 Larson AG, Elnatan D, Keenen MM, et al. Liquid droplet formation by HP1α suggests a role for phase separation in heterochromatin. Nature 2017;547:236–240.
54 Lieberman-Aiden E, van Berkum NL, Williams L, et al. Comprehensive mapping of long-range interactions reveals folding principles of the human genome. Science (80-) 2009;326:289–293.
55 Heinz S, Benner C, Spann N, et al. Simple combinations of lineage-determining transcription factors prime cis-regulatory elements required for macrophage and B cell identities. Mol Cell 2010;38:576–589.
56 Pope BD, Ryba T, Dileep V, et al. Topologically associating domains are stable units of replication-timing regulation. Nature 2014;515:402–405.
57 Sud'ina GF, Galkina SI, Margolis LB, et al. Dependence of neutrophil activation on cell density and adhesion. Cell Adhes Commun 1998;5:27–37.
58 Mitchell MJ, Lin KS, King MR. Fluid shear stress increases neutrophil activation via platelet-activating factor. Biophys J 2014;106:2243–2253.
59 Pertega-Gomes N, Vizcaino JR, Felisbino S, et al. Epigenetic and oncogenic regulation of SLC16A7 (MCT2) results in protein over-expression, impacting on signalling and cellular phenotypes in prostate cancer. Oncotarget 2015;6:21675–21684.
60 Fisel P, Kruck S, Winter S, et al. DNA methylation of the SLC16A3 promoter regulates expression of the human lactate transporter MCT4 in renal cancer with consequences for clinical outcome. Clin Cancer Res 2013;19:5170–5181.
61 Kramer PA, Ravi S, Chacko B, et al. A review of the mitochondrial and glycolytic metabolism in human platelets and leukocytes: Implications for their use as bioenergetic biomarkers. Redox Biol 2014;2:206–210.
62 Mookerjee SA, Brand MD. Measurement and analysis of extracellular acid production to determine glycolytic rate. J Vis Exp 2015:e53464.
63 Cao S, Liu P, Zhu H, et al. Extracellular acidification acts as a key modulator of neutrophil apoptosis and functions. PLoS One 2015;10:e0137221.
64 Verdone JE, Zarif JC, Pienta KJ. Aerobic glycolysis, motility, and cytoskeletal remodeling. Cell Cycle 2015;14:169–170.
65 Stenmark H. Rab GTPases as coordinators of vesicle traffic. Nat Rev Mol Cell Biol 2009;10:513–525.
66 Faurschou M, Borregaard N. Neutrophil granules and secretory vesicles in inflammation. Microbes Infect 2003;5:1317–1327.
67 Sheshachalam A, Srivastava N, Mitchell T, et al. Granule protein processing and regulated secretion in neutrophils. Front Immunol 2014;5:448.
68 Hanlon WA, Stolk J, Davies P, et al. rTNF alpha facilitates human polymorphonuclear leukocyte adherence to fibrinogen matrices with mobilization of specific and tertiary but not azurophilic granule markers. J Leukoc Biol 1991;50:43–48.
69 Xu X, Håkansson L. Degranulation of primary and secondary granules in adherent human neutrophils. Scand J Immunol 2002;55:178–188.
70 McLeish KR, Merchant ML, Creed TM, et al. Frontline Science: Tumor necrosis factor-α stimulation and priming of human neutrophil granule exocytosis. J Leukoc Biol 2017;102:19–29.
71 Sengeløv H, Follin P, Kjeldsen L, et al. Mobilization of granules and secretory vesicles during in vivo exudation of human neutrophils. J Immunol 1995;154:4157–4165.
72 Strom AR, Emelyanov A V., Mir M, et al. Phase separation drives heterochromatin domain formation. Nature 2017;547:241–245.
73 Hyman AA, Weber CA, Jülicher F. Liquid-liquid phase separation in biology. Annu

Rev Cell Dev Biol 2014;30:39–58.
74 Denais CM, Gilbert RM, Isermann P, et al. Nuclear envelope rupture and repair during cancer cell migration. Science 2016;352:353–358.
75 Raab M, Gentili M, de Belly H, et al. ESCRT III repairs nuclear envelope ruptures during cell migration to limit DNA damage and cell death. Science 2016;352:359–362.
76 Mifsud B, Tavares-Cadete F, Young AN, et al. Mapping long-range promoter contacts in human cells with high-resolution capture Hi-C. Nat Genet 2015;47:598–606.
77 Danko CG, Hyland SL, Core LJ, et al. Identification of active transcriptional regulatory elements from GRO-seq data. Nat Methods 2015;12:433–438.
78 Sanna T, Dello Russo A, Toniolo D, et al. Cardiac features of Emery–Dreifuss muscular dystrophy caused by lamin A/C gene mutations. Eur Heart J 2003;24:2227–2236.
79 Yoon Y-S, Park J-S, Tkebuchava T, et al. Unexpected severe calcification after transplantation of bone marrow cells in acute myocardial infarction. Circulation 2004;109:3154–3157.
80 Bloom S, Peric-Golia L. Geographic variation in the incidence of myocardial calcification associated with acute myocardial infarction. Hum Pathol 1989;20:726–731.
81 Lei K, Zhang X, Ding X, et al. SUN1 and SUN2 play critical but partially redundant roles in anchoring nuclei in skeletal muscle cells in mice. Proc Natl Acad Sci U S A 2009;106:10207–10212.
82 Chen C-Y, Chi Y-H, Mutalif RA, et al. Accumulation of the inner nuclear envelope protein Sun1 Is pathogenic in progeric and dystrophic laminopathies. Cell 2012;149:565–577.
83 Olins AL, Hoang T V., Zwerger M, et al. The LINC-less granulocyte nucleus. Eur J Cell Biol 2009;88:203–214.
84 Mark Welch DB, Jauch A, Langowski J, et al. Transcriptomes reflect the phenotypes of undifferentiated, granulocyte and macrophage forms of HL-60/S4 cells. Nucleus 2017;8:222–237.
85 Rao SSP, Huntley MH, Durand NC, et al. A 3D map of the human genome at kilobase resolution reveals principles of chromatin looping. Cell 2014;159:1665–1680.

Declarations

Ethics approval and consent to participate

Not Applicable

Consent for publication

Not Applicable

Availability of data and materials

The datasets generated and analysed during the current study are available in the GEO repository, accession number xxxxx. Scripts and data to reproduce analysis of processed data is available on github url: xxxxx. Additional unfiltered results tables are available on Figshare: xxxxx

Competing interests

The authors declare that they have no competing interests

Funding
This research was supported by a Health Research Council Explorer grant (HRC 15/604) to JMO. ECJ was recipient of an University of Auckland doctoral scholarship, and Maurice Wilkins Centre travel grant. The funding bodies had no role in the study design, collection, analysis, and interpretation of the data, or preparing the manuscript.

Authors' Contributions
All authors contributed to conception and design of the study. ECJ performed the experiments, analysed and interpreted the data, and wrote the manuscript with support from JMO, JKP, and MHV. All authors contributed to revisions and approved the final manuscript.

Acknowledgements
The authors would like to thank Peter Shepherd and the members of the JMO lab group for comments and discussion. We thank Jacqueline Ross in the Biomedical Imaging Research Unit, University of Auckland for assistance with developing the assay, and Stephen Edgar in the Core Flow Cytometry Facility, FMHS, University of Auckland for assistance with flow cytometry.

Additional files

Additional File 1: Figures S1-S4. S1. HL60 cells differentiated into neutrophil-like cells and migrated through two pore sizes. **S2.** SEM of porous membranes. **S3.** Genome organisation changes after migration through two pore sizes. **S4.** RNA-seq PCA plot.

Additional File 2: Table S1. *Significantly differentially expressed genes*. All genes with significantly differential gene expression (FDR<0.05) between either 5µm pores compared to control, 14µm pores compared to control, or 5µm pores compared to 14µm pores. Sets refer to those described on page 4 (*Transcriptional changes after migration and remodelling are distinct*). HUGO gene names, Ensembl gene names and IDs are provided as identifiers. Columns suffixed with '_5' represent results from 5µm pore compared to control. Columns suffixed with '_14' represent results from 14µm pore compared to control. Columns suffixed with '_5v14' represent results from 5µm pore compared to 14µm pore. The 'padj' shows the FDR adjusted p-value.

Additional File 3: Table S2-S5, S8-S10. S2. Gene ontology enrichment (Biological process) of Figure 2B. **S3.** Gene ontology enrichment (Biological process) of Figure 2C. **S4.** Gene ontology enrichment (Biological process) of Figure 2D. **S5.** Gene ontology enrichment (Molecular function) of Figure 2D. **S8.** RNA-seq QC. **S9.** HiCUP QC. **S10.** Hi-C replicate correlations.

Additional File 4: Table S6. *Correlation between the interaction patterns of 300kb bins.* Each 300kb bin has an interaction pattern with every other bin in the chromosome. When these interactions patterns are correlated between experiments, anticorrelation indicates a switch in interaction pattern and thus a change from one compartment to the other. Calculated using the getHiCcorrDiff.pl in HOMER.

Additional File 5: Table S7. *Genes in disrupted contacts.* All genes in contacts that significantly decrease in frequency in 5µm pores compared to control cells.

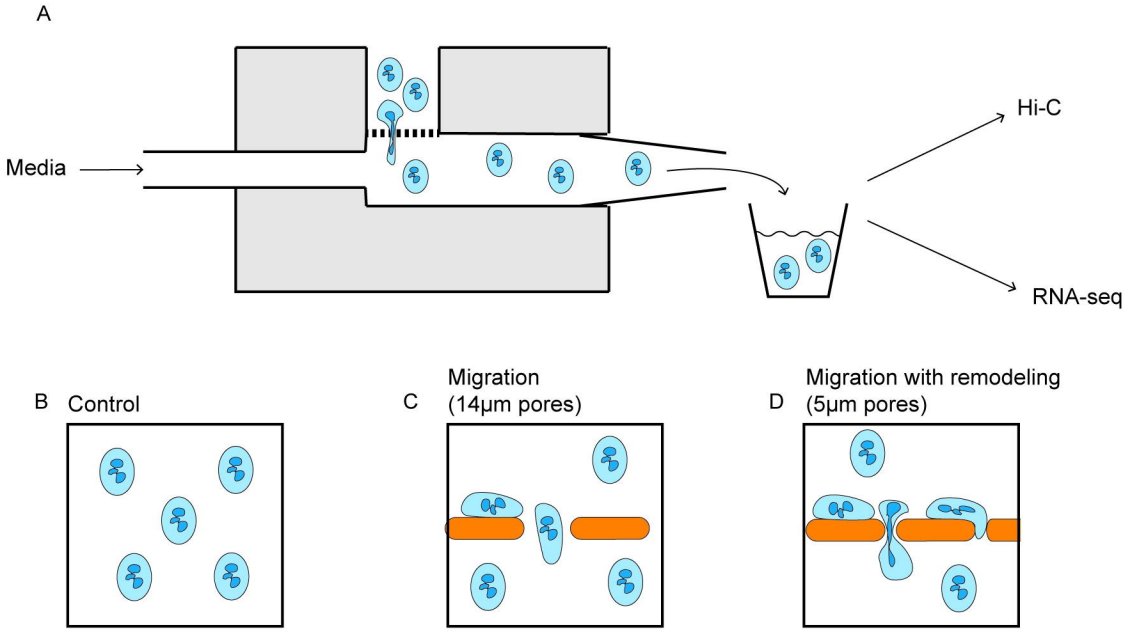
A
Media
Hi-C
RNA-seq
B
Control
C
Migration
(14μm pores)
D
Migration with remodeling
(5μm pores)

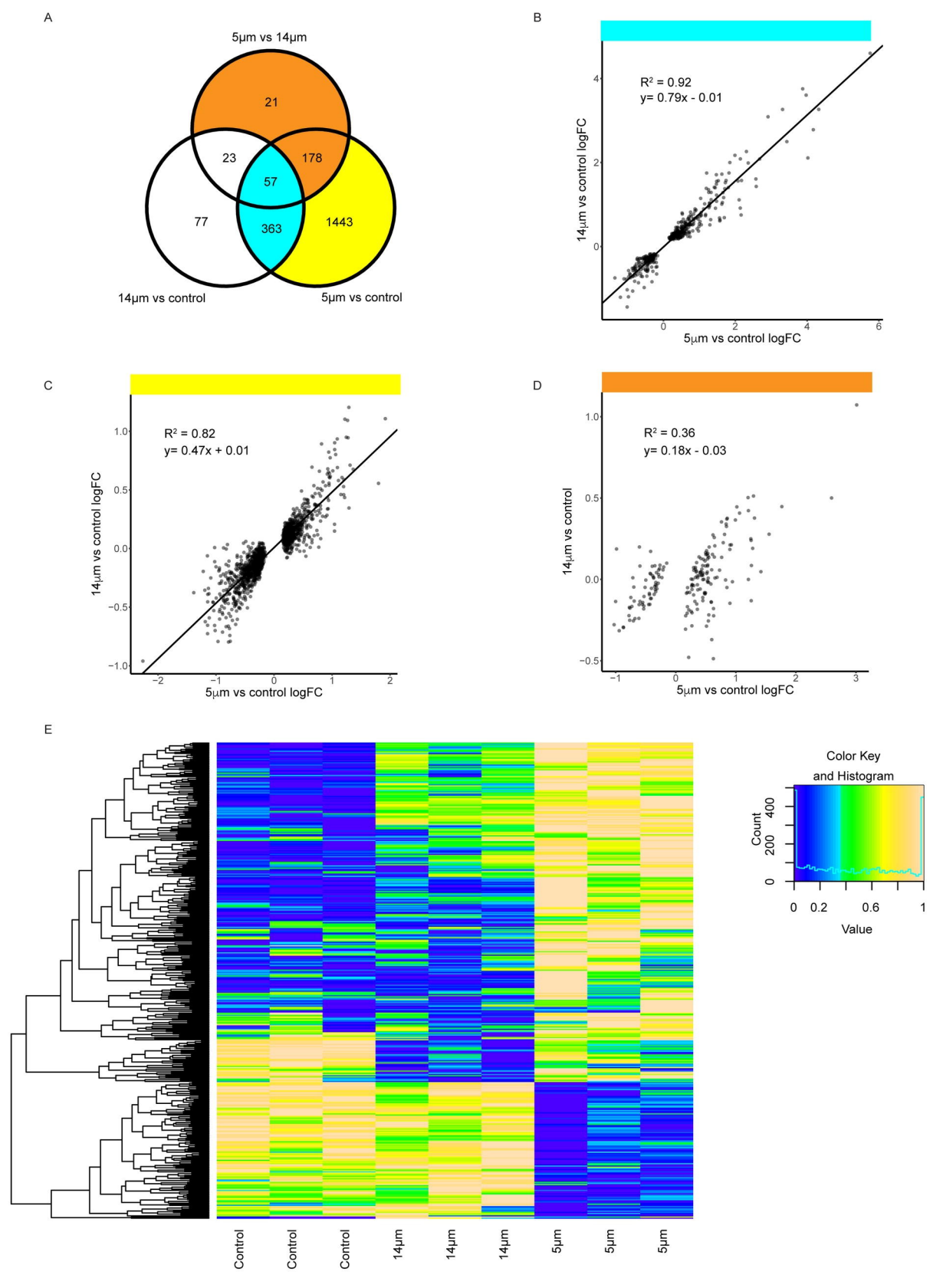
A
5μm vs 14μm
21
23
178
57
77
363
1443
14μm vs control
5μm vs control
B
R² = 0.92
y= 0.79x - 0.01
14μm vs control logFC
5μm vs control logFC
C
R² = 0.82
y= 0.47x + 0.01
14μm vs control logFC
5μm vs control logFC
D
R² = 0.36
y= 0.18x - 0.03
14μm vs control
5μm vs control logFC
E
Color Key
and Histogram
Count
Value
Control
Control
Control
14μm
14μm
14μm
5μm
5μm
5μm

A

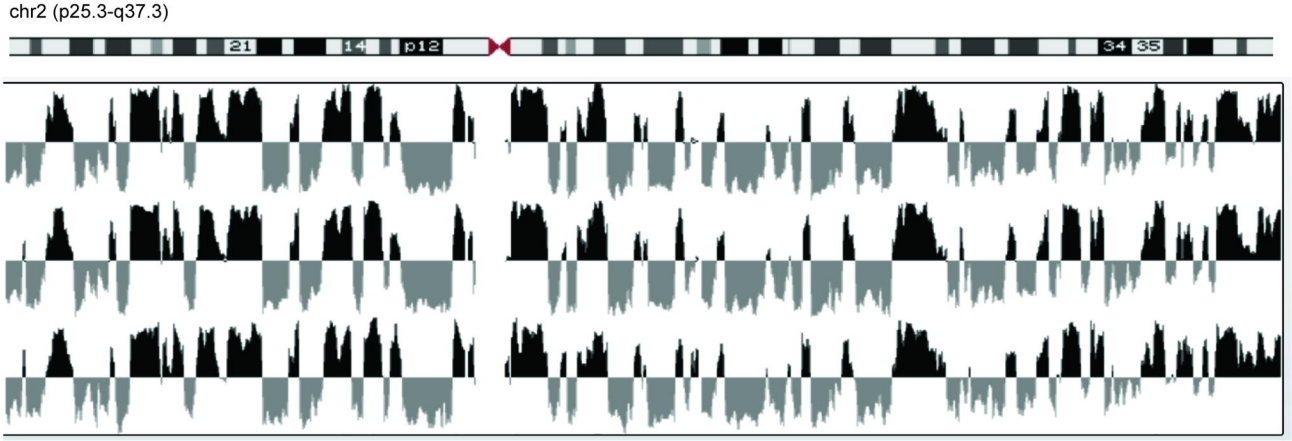
chr2 (p25.3-q37.3)
21
14
p12
34
35
i
ii
iii

B

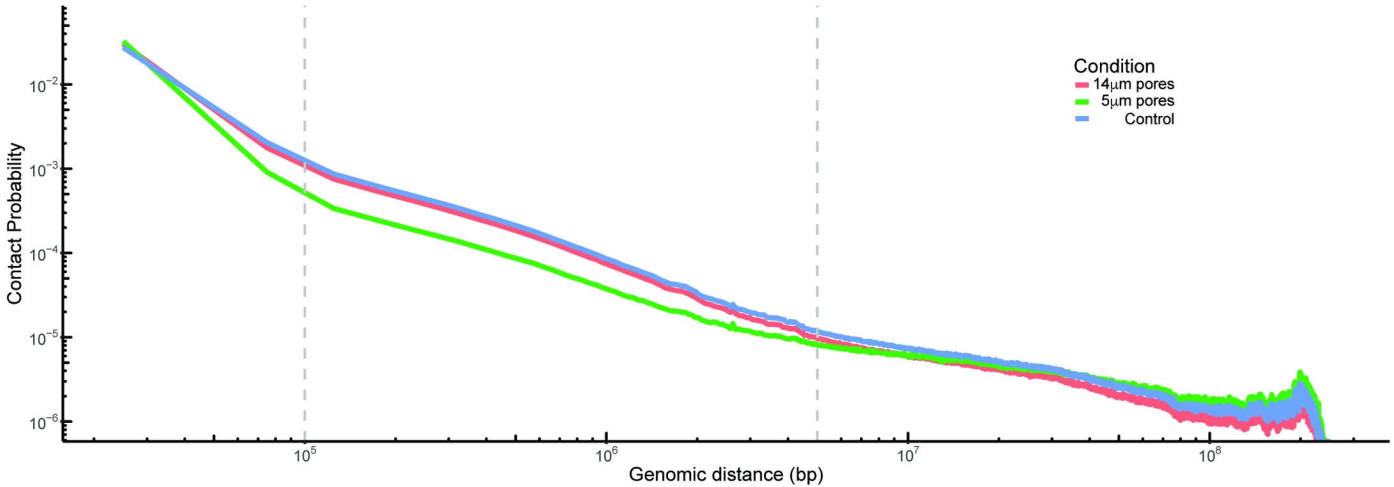
Condition
14μm pores
5μm pores
Control
Contact Probability
10^{-2}
10^{-3}
10^{-4}
10^{-5}
10^{-6}
10^{5}
10^{6}
10^{7}
10^{8}
Genomic distance (bp)

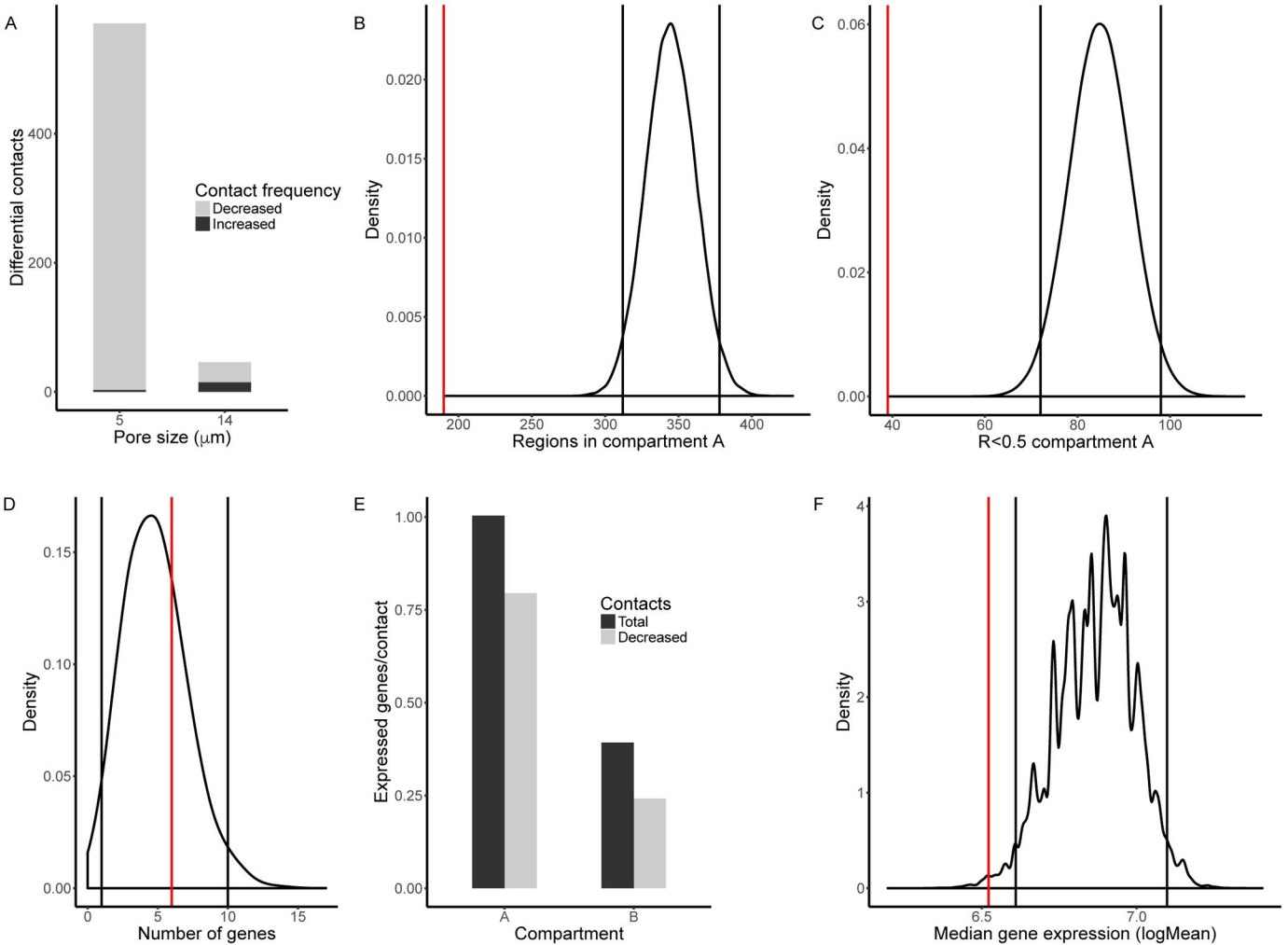
A
Differential contacts
400
200
0
Contact frequency
Decreased
Increased
5
14
Pore size (μm)
B
Density
0.020
0.015
0.010
0.005
0.000
200
250
300
350
400
Regions in compartment A
C
Density
0.06
0.04
0.02
0.00
40
60
80
100
R<0.5 compartment A
D
Density
0.15
0.10
0.05
0.00
0
5
10
15
Number of genes
E
Expressed genes/contact
1.00
0.75
0.50
0.25
0.00
Contacts
Total
Decreased
A
B
Compartment
F
Density
4
3
2
1
0
6.5
7.0
Median gene expression (logMean)

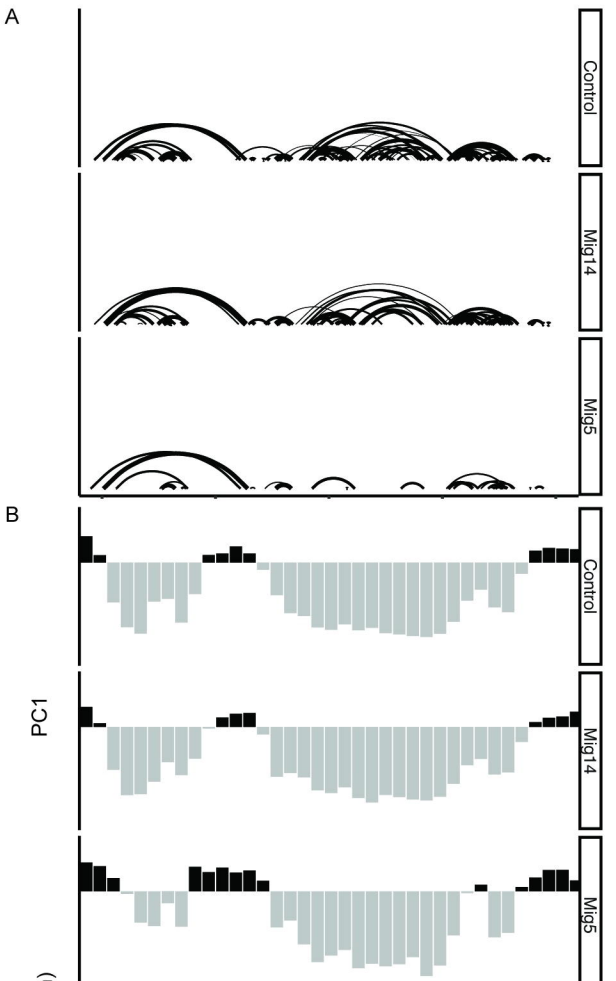
A
Control
Mig14
Mig5
B
PC1
Control
Mig14
Mig5
C
log(baseMean)
65000000
67500000
70000000
72500000
75000000
Chromosome 17